JCI insight

RESEARCH ARTICLE

CXCR3 regulates CD4+ T cell cardiotropism in pressure overload–induced cardiac dysfunction

Njabulo Ngwenyama,[1] Ane M. Salvador,[1] Francisco Velázquez,[1] Tania Nevers,[1] Alexander Levy,[2] Mark Aronovitz,[2] Andrew D. Luster,[3] Gordon S. Huggins,[2] and Pilar Alcaide[1]

[1]Department of Immunology and [2]Molecular Cardiology Research Institute Tufts University, Boston, Massachusetts, USA. [3]Division of Rheumatology, Allergy and Immunology, Center for Immunology and Inflammatory Diseases, Massachusetts General Hospital, Harvard Medical School, Boston, Massachusetts, USA.

Heart failure (HF) is associated in humans and mice with increased circulating levels of CXCL9 and CXCL10, chemokine ligands of the CXCR3 receptor, predominantly expressed on CD4+ Th1 cells. Chemokine engagement of receptors is required for T cell integrin activation and recruitment to sites of inflammation. Th1 cells drive adverse cardiac remodeling in pressure overload–induced cardiac dysfunction, and mice lacking the integrin ligand ICAM-1 show defective T cell recruitment to the heart. Here, we show that CXCR3+ T cells infiltrate the heart in humans and mice with pressure overload–induced cardiac dysfunction. Genetic deletion of CXCR3 disrupts CD4+ T cell heart infiltration and prevents adverse cardiac remodeling. We demonstrate that cardiac fibroblasts and cardiac myeloid cells that include resident and infiltrated macrophages are the source of CXCL9 and CXCL10, which mechanistically promote Th1 cell adhesion to ICAM-1 under shear conditions in a CXCR3-dependent manner. To our knowledge, our findings identify a previously unrecognized role for CXCR3 in Th1 cell recruitment into the heart in pressure overload–induced cardiac dysfunction.

Introduction

The complex syndrome of heart failure (HF) is currently the leading cause of mortality and hospitalization in the US and is associated with a very poor prognosis (1). HF develops as a result of a variety of pathological stimuli that can be ischemic and nonischemic in nature, leading to increased left ventricular (LV) pressures and the inability of the heart to pump blood efficiently and maintain adequate perfusion of tissues (2). Regardless of the etiology, rapid and sustained induction of inflammatory chemokines, cytokines, and adhesion molecules is thought to be critical for mediating leukocyte recruitment into the heart that results in cardiac inflammation associated with cardiac dysfunction and HF (3–8). Among these, CXCL9 (MIG), CXCL10 (IP-10), and CXCL11 (I-TAC) — the ligands of the chemokine receptor CXCR3 — and the adhesion molecule ICAM-1 have all been associated systemically with the progression of HF in patients (9–12). Whether these are directly responsible for heart inflammation and cardiac dysfunction remains unresolved and requires further mechanistic investigation.

CXCR3 is a GPCR expressed mainly by CD4+ Th1 cells. Its expression is regulated by T-bet, the signature Th1 cell transcription factor, and signaling through CXCR3 induces Th1 cell–driven inflammation (13). CXCR3 is also expressed by other immune cells such as CD8+ cytotoxic T cells, NK cells, NK T cells, plasmacytoid DCs (pDC), and a recently described subset of Tregs and — to a minor extent — by nonimmune cells that include cardiac fibroblasts, vascular smooth muscle cells, and endothelial cells (14–16). Rapid engagement of CXCR3 by its ligands results in T cell adhesion to human ICAM-1 and human endothelial cells and induces transendothelial migration in vitro, through mechanisms that involve changes in T cell integrin affinity for its ligand ICAM-1 (17–19). Thus, in vivo, release of CXCR3 ligands in inflamed tissues likely mediates Th1 cell recruitment and inflammation through mechanisms that involve ICAM-1 (17, 20), but this has yet to be established in vivo in T cell–mediated cardiac inflammation.

Several recent studies using mouse experimental models of heart inflammation, including our own, have described a critical role for CD4+ T cells in the heart and positioned them as central players in adverse cardiac remodeling associated with cardiac dysfunction and HF (3, 4, 21). The CD4+ T cell subset involved

Authorship note: NN and AMS contributed equally to this work.

Conflict of interest: The authors have declared that no conflict of interest exists.

Submitted: October 11, 2018
Accepted: February 14, 2019
Published: April 4, 2019.

Reference information: *JCI Insight*. 2019;4(7):e125527. https://doi.org/10.1172/jci.insight.125527.

and the kinetics of recruitment to the heart appear to differ in response to ischemic vs. nonischemic insults. For instance, $CD4^+$ T cells are necessary for healing after ischemia; however, Th1 cells, the main T cell subset expressing CXCR3, are not prevalent in the heart in chronic ischemic HF (22). Moreover, the CXCR3 ligand CXCL10 is critical in the reparative response after ischemia but through mechanisms that are independent of CXCR3 regulation of immune cell recruitment (15). A similar role for CXCL10 was also reported in the bleomycin experimental model of lung inflammation and fibrosis (23). In contrast, $CD4^+$ T cells — and, more specifically, Th1 cells — are predominantly recruited to the heart and drive cardiac fibrosis and dysfunction in response to cardiac pressure overload. Moreover, ICAM-1 deficiency results in decreased T cell infiltration in the heart and prevents adverse cardiac remodeling and cardiac dysfunction (3–5, 21). While *Cxcl9* and *Cxcl10* transcripts have been reported to be elevated in the heart in response to cardiac pressure overload (9), the cellular source, the question of whether they induce signals through CXCR3 that lead to Th1 cell recruitment to the heart, and the mechanisms involved in T cell cardiotropism need to be further explored. Understanding such mechanistic actions in different inflammatory settings in the heart is critical to effectively treat HF resulting from different etiologies in which specific heart inflammatory mechanisms take place.

Here, in an effort to investigate the mechanisms of Th1 cell cardiotropism in pressure overload–induced cardiac dysfunction, we hypothesized that cardiac resident cells release CXCL9 and CXCL10, which targets $CXCR3^+$ Th1 cells and mediate ICAM-1–dependent recruitment to the heart. We report the potentially novel finding that CXCL9 and CXCL10 chemokines produced by cardiac myeloid cells and fibroblasts induce $CXCR3^+$ T cell cardiotropism and adverse cardiac remodeling by mechanisms that involve T cell integrin activation and adhesion to ICAM-1.

Results

Cardiac $CXCR3^+$ T cells are present in nonischemic HF patients and in mice in response to cardiac pressure overload–induced by transverse aortic constriction (TAC). Circulating levels of the CXCR3 chemokine ligands CXCL9 and CXCL10 are elevated during adverse cardiac remodeling in humans as well as in the murine TAC model of pressure overload–induced HF (24, 25), characterized by T cell infiltration in the heart (4, 21). We first sought to evaluate the expression of CXCR3 in LV tissue from human end-stage nonischemic HF subjects by IHC. Compared with non-HF controls, nonischemic HF subjects showed a significantly greater presence of LV $CXCR3^+$ cells, particularly in leukocyte-rich areas (Figure 1, A and B). Additional studies using immunofluorescence and costaining with anti-CXCR3 and anti-CD3 antibodies demonstrated a significant number of $CD3^+CXCR3^+$ T cells in the LV of nonischemic HF patients, in contrast to the LV of non-HF controls. While the majority of the $CXCR3^+$ cells in the LV were T cells, our studies also identified non–T cell $CXCR3^+$ cells in the human LV from patients with HF (Figure 1, C and D). In mice with cardiac pressure overload induced by TAC, we detected a significant increase in the number of LV myocardial $CXCR3^+CD4^+$ T cells, as compared with Sham-operated control mice, and these cells expressed the integrin LFA-1, the main T cell ligand for ICAM-1 (Figure 1, E and F). We hypothesized that the CXCR3 ligands CXCL9 and CXCL10 are induced in the heart and promote $CXCR3^+CD4^+$ T cell cardiotropism. Because C57BL/6 mice do not express CXCL11 (26), the only CXCR3 chemokines analyzed in these murine studies were CXCL9 and CXCL10. Mice were subjected to TAC and Sham surgery and the expression kinetics of *Cxcl9* and *Cxcl10* in the LV was evaluated over time by quantitative PCR (qPCR). mRNA expression of both CXCR3 ligands *Cxcl9* and *Cxcl10* was sequentially increased to a similar extent in the LV of TAC mice as compared with Sham mice (Figure 1, G and H). The mRNA levels of *Ifng* and *Tnfa*, known to induce *Cxcl9* and *Cxcl10* expression in various cell types (14), followed similar expression kinetics as *Cxcl9* and *Cxcl10* (Figure 1, I and J). Taken together, the presence of $CXCR3^+$ T cells is increased in the heart of humans and mice with pressure overload–induced cardiac dysfunction. In mice, the expression of *Cxcl9* and *Cxcl10*, and the cytokines known to induce them such as *Ifng* and *Tnfa*, parallels the time course of $CD4^+$ T cell infiltration, as we have previously described (4).

CXCL9 and CXCL10 are produced by cardiac myeloid cells and cardiac fibroblasts in response to cardiac pressure overload. The CXCR3 ligands CXCL9 and CXCL10 have been shown to be secreted by several cell types including monocytes, macrophages, fibroblasts, and endothelial cells upon stimulation with proinflammatory cytokines (14, 15, 27). All of these cells are present in the heart and could be the chemokine source that triggers the recruitment of $CXCR3^+CD4^+$ T cells to the heart. To determine the cardiac cells expressing these chemokines in response to cardiac pressure overload, we subjected Reporting the Expression of CXCR3 Ligands (REX3) mice to TAC. REX3 mice express red fluorescent protein (RFP) and blue fluorescent protein (BFP) under the

Cxcl9 and *Cxcl10* promoters, respectively, and allow for the examination of *Cxcl9* and *Cxcl10* gene expression in vivo (13). LV tissues of Sham- and TAC-operated mice were harvested 1 week and 4 weeks after surgery, and the expression of RFP and BFP was visualized by immunofluorescence and quantified by flow cytometry. While the LV of Sham-operated mice was devoid of *Cxcl9* and *Cxcl10* reporter expression, reporter fluorescence could easily be identified by immunofluorescence in TAC operated mice after 4 weeks (Figure 2, A–C). CXCL10 was identified in nonfibrotic areas and mainly colocalized with $CD45^+$ leukocytes (Figure 2B), but not with $CD31^+$ endothelial cells (Figure 2C) or with cardiomyocytes outlined with wheat germ agglutinin (WGA) (Figure 2A). Interestingly, cells localized between the cardiomyocytes that were $CD45^-$ were also identified as producers of CXCL10. In contrast, the expression of CXCL9 in nonfibrotic areas was very low in TAC mice. In areas of fibrosis (also stained with WGA) and leukocytic infiltration ($CD45^+$), CXCL10-expressing cells were increased, while CXCL9 expression became more evident. Both CXCL9 and CXCL10 were mainly colocalized with CD45 and with WGA^+ staining surrounding the cardiomyocytes — but not with cardiomyocytes themselves or $CD31^+$ endothelial cells (Figure 2, A–C). Thus, both $CD45^+$ leukocytes as well as $CD45^-$ cell types, not identified as endothelial cells or cardiomyocytes, expressed CXCL9 and CXCL10 in the heart; whereas CXCL9 was only expressed in fibrotic areas, CXCL10 was expressed more broadly with a higher expression observed in areas of fibrosis. To more comprehensively delineate the CXCL9 and CXCL10 cell source in the LV, and to quantify the temporal cell–specific chemokine expression, we used flow cytometry in the LV 1 week and 4 weeks after TAC, before and after significant T cell infiltration and cardiac remodeling occur, respectively. As expected, we identified $CD3^+$ T cells and $CD11b^+$ myeloid cells within the $CD45^+$ leukocyte cellular compartment. $CD3^+$ T cells were in very low numbers 1 week after TAC and significantly increased 4 weeks after TAC, and CXCL9 and CXCL10 were undetectable in T cells at both time points (Figure 2, E–J). We gated endothelial cells labeled as $CD31^+CD45^-$ and used the recently reported antibody MEFSK4 to label and gate cardiac fibroblasts as $MEFSK4^+CD45^-$ cells (Figure 2D) (28). At 1 week after TAC, no CXCL9 expression was detected, and CXCL10 expression was exclusively detected in myeloid cells (Figure 2, E–G). At 4 weeks after TAC, in support of our histological findings, cardiac myeloid cells expressed the highest levels of both CXCL9 and CXCL10, with CXCL10 being expressed to a higher extent (Figure 2, H–J). Interestingly, $MEFSK4^+$ cardiac fibroblasts were also identified as both CXCL9 and CXCL10 producers at 4 weeks after TAC, whereas T cells or endothelial cells were not. Taken together, these data indicate that 1 week after cardiac pressure overload is induced, when adverse cardiac remodeling is not evident, CXCL10 is the only chemokine ligand of CXCR3 expressed in the heart, and it is specifically expressed by cardiac myeloid cells. Later, 4 weeks after TAC — when T cell infiltration, adverse cardiac remodeling, and cardiac dysfunction is evident — CXCL10 and, to a lesser extent, CXCL9 are expressed by cardiac myeloid cells as well as cardiac fibroblasts in response to cardiac pressure overload.

CXCL9 and CXCL10 are expressed by resident and recruited cardiac myeloid cells in response to cardiac pressure overload. During cardiac pressure overload, several subsets of myeloid cells can be detected in the heart. These include neutrophils and monocytes, as well as resident and recruited macrophages. To determine the specific cardiac myeloid cell types expressing CXCL9 and CXCL10 chemokines in response to cardiac pressure overload, we subjected REX3 mice to TAC surgery and harvested LV tissue at 4 weeks after surgery. Flow cytometry was used to comprehensively delineate the specific myeloid cell source of CXCL9 and CXCL10 in the LV and to quantify cell-specific chemokine expression in $CD45^+CD11b^+Ly6G^+$ neutrophils, $CD45^+CD11b^+MerTK^-CCR2^+$ recruited monocytes, $CD45^+CD11b^+MerTK^+CCR2^+$ recruited macrophages, and $CD45^+CD11b^+MerTK^+CCR2^-$ resident macrophages (Figure 3, A and B). The percentages and absolute numbers of each myeloid cell subset expressing CXCL9 and CXCL10 was quantified (Figure 3, C–F). $CCR2^+$ recruited monocytes and macrophages, as well as $CCR2^-$ resident macrophages, expressed CXCL10 with the greatest frequency, while CXCL9 was mainly expressed by a high percentage of $CCR2^+$ recruited macrophages (Figure 3, C and D). When absolute numbers of cells in the LV were analyzed, cardiac resident macrophages were identified as the dominant cells expressing both CXCL9 and CXCL10, in significantly greater numbers than the other myeloid cell subsets evaluated (Figure 3, E and F). Taken together, these data indicate that CXCL9 and CXCL10 are produced predominantly by cardiac resident macrophages in response to cardiac pressure overload to a lesser extent by LV recruited monocytes and macrophages, and they demonstrate that neutrophils are not a source of CXCL9 or CXCL10.

$CXCR3^+CD4^+$ T cells are expanded in the cardiac draining lymph nodes in response to cardiac pressure overload and express high levels of LFA-1. The mediastinal lymph nodes (mLN) are the secondary lymphoid organ where a $CD4^+$ T cell response is initiated after TAC, and this response is characterized by specific expansion of

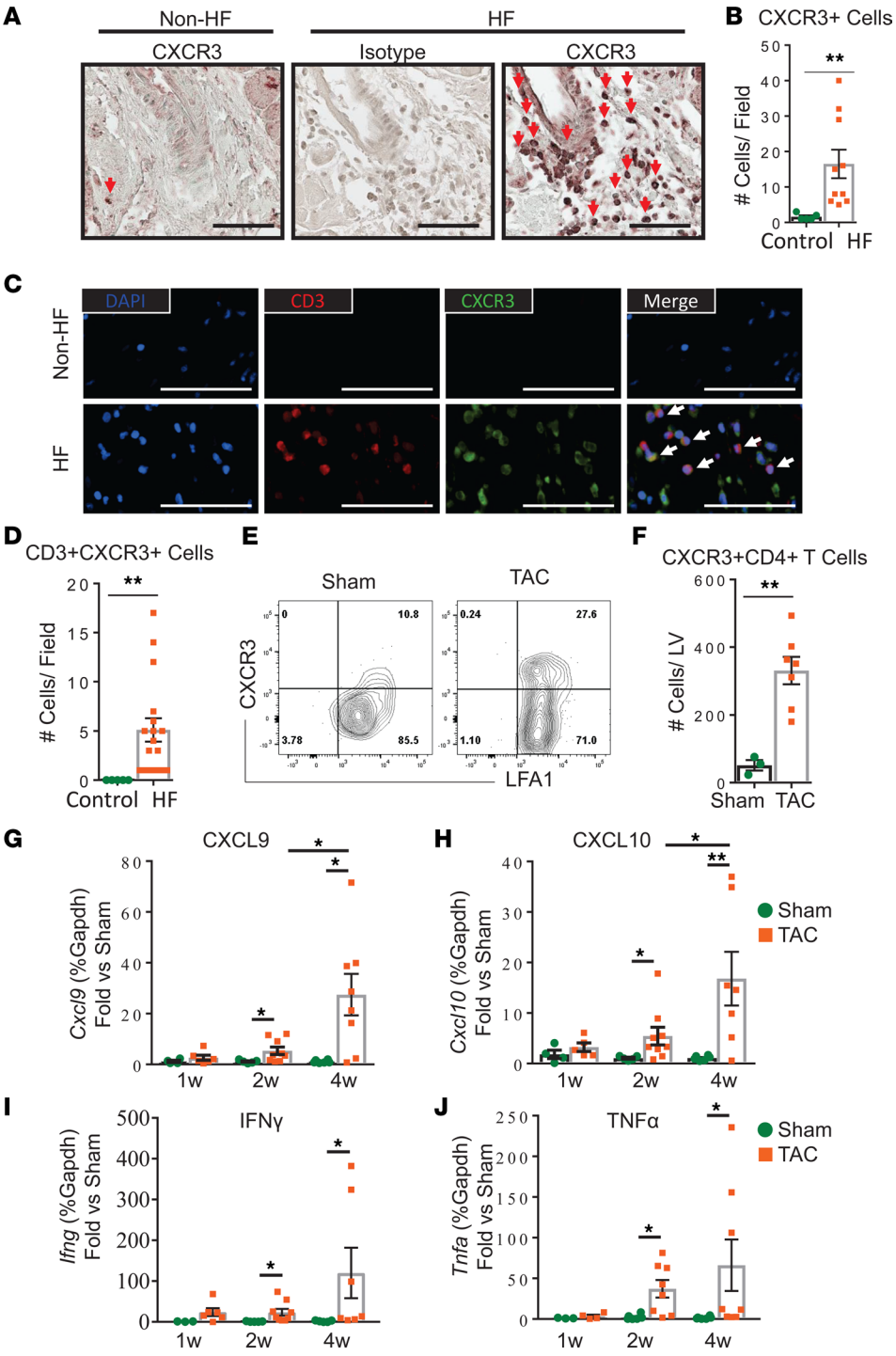

Figure 1. CXCR3⁺ T cell infiltration in humans and mice with cardiac pressure overload. (**A** and **B**) LV tissue sections from non-HF or nonischemic HF human subjects were stained for CXCR3 or isotype control by IHC (representative CXCR3⁺ leukocyte–shaped cells are indicated with red arrows) (**A**) and quantified in multiple fields of view using a 40× objective (**B**). (**C** and **D**) LV tissue sections were stained for DAPI (blue), CD3 (red), and CXCR3 (green) by immunofluorescence (**C**), and the number of cells showing colocalization were quantified in multiple fields of view per section using a 40× objective (**D**). Scale bar: 100 μm. n = 2 control, 3 HF. Error bars represent mean ± SEM (**P < 0.01; Mann-Whitney unpaired U test). (**E** and **F**) CD4⁺ T cells isolated from the LV tissue of mice 4 weeks after Sham or TAC surgery were analyzed (**E**) and quantified (**F**) for surface CXCR3 and LFA-1 expression within the CD4⁺ gate by flow cytometry. n = 3 Sham, 7 TAC. Error bars represent mean ± SEM (**P < 0.01; Mann-Whitney unpaired U test). (**G–J**) Chemokine and cytokine mRNA levels in the LV of WT mice at different time points after surgery were determined by qPCR for *Cxcl9* (**G**), *Cxcl10* (**H**), *Ifng* (**I**), and *Tnfa* (**J**). n = 4 Sham, 5 TAC 1 weeks (w); 5 Sham, 9 TAC 2w; 6 Sham, 8 TAC 4w. Error bars represent mean ± SEM (*P < 0.05, **P < 0.01; 1-way ANOVA with Bonferroni post hoc test).

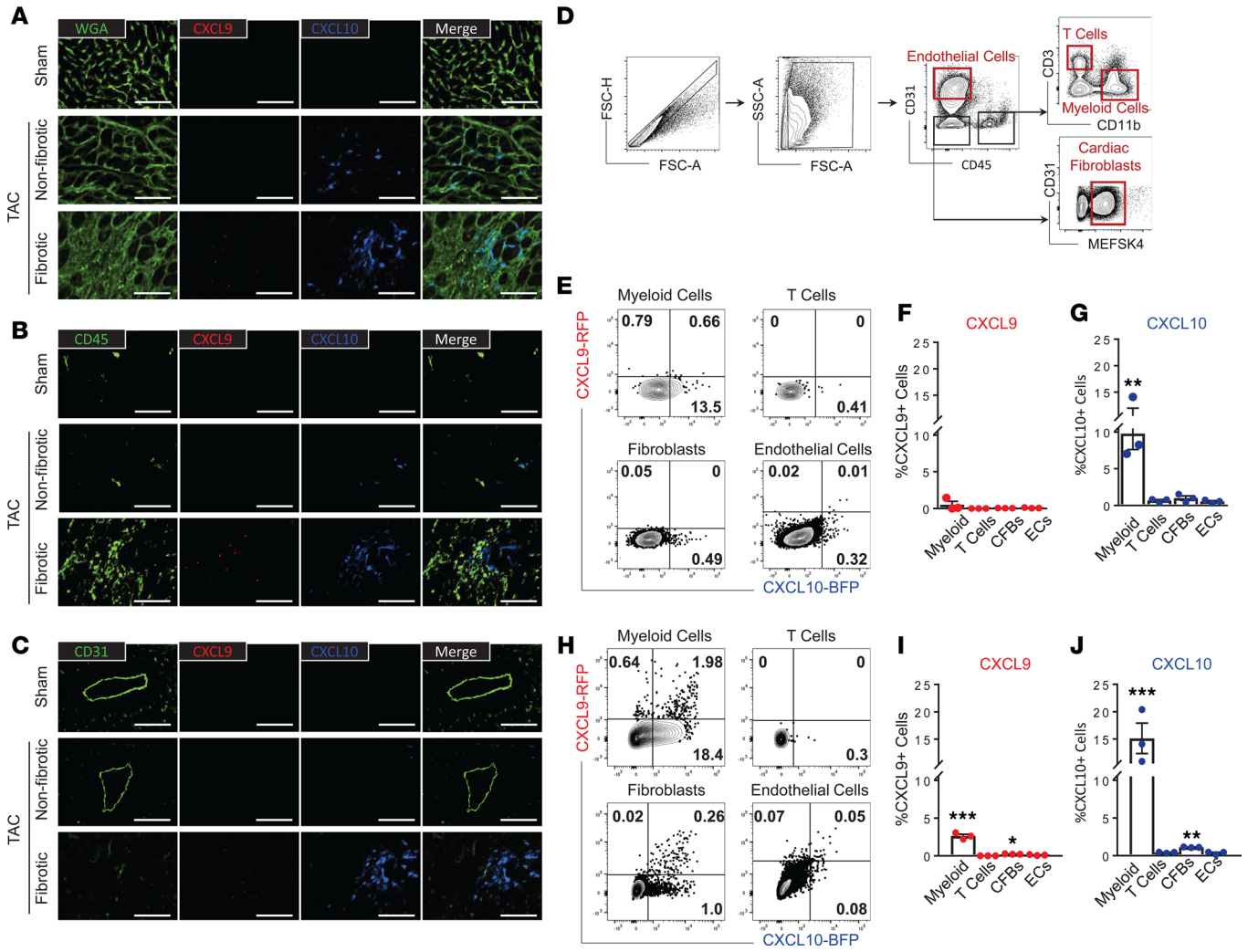

Figure 2. CXCL9 and CXCL10 are produced by cardiac myeloid cells and fibroblasts in response to cardiac pressure overload. REX3 mice were subjected to Sham and TAC surgery, and LV tissue sections were isolated for analysis of CXCL9 and CXCL10 expression by immunofluorescence. (**A–C**) The outline of cardiomyocytes was identified by wheat germ agglutinin (WGA) staining (**A**), leukocytes were identified with anti-CD45 (**B**), and endothelial cells identified with anti-CD31 (**C**) in Sham mice (top row) and TAC mice 4 weeks after surgery in nonfibrotic areas (middle row) and fibrotic areas (bottom row), also stained by WGA. Scale bars: 100 μm. *n* = 3 mice per group. (**D–J**) Cardiac endothelial cells (ECs), myeloid cells, T cells, and cardiac fibroblasts (CFBs) were identified by flow cytometry with the indicated gating strategy (**D**), to quantify the frequency of CXCL9- and CXCL10-producing cells 1 week after TAC surgery (**E–G**) and 4 weeks after TAC surgery (**H–J**). Statistical comparisons are indicated compared with ECs. *n* = 3 mice per group. Error bars represent mean ± SEM (**P* < 0.05, ***P* < 0.01, ****P* < 0.001; 1-way ANOVA with Bonferroni post hoc test).

$CD4^+IFN\gamma^+$ Th1 cells (3, 4, 21). Th1 differentiation is under the control of the transcription factor T-bet, which has also been reported to regulate the expression of CXCR3. Thus, we next tested whether and when $CXCR3^+CD4^+$ T cell expansion occurred in the cardiac draining LNs. $CXCR3^+CD4^+$ T cells were increased in the mLNs at 1 week after TAC, before $CD4^+$ T cell LV infiltration occurs, as we have previously described (4), and sequentially increased at later time points after TAC when T cells can also be found infiltrated in the heart. This expansion was not observed in Sham-operated mice (Figure 4A). Remarkably, all $CXCR3^+CD4^+$ T cells expressed high levels of total LFA-1, the ligand for ICAM-1, and this was also increased over time (Figure 4, A and B). Moreover, $CXCR3^+CD4^+$ T cells expressed significantly higher levels of total LFA-1 than $CXCR3^-CD4^+$ T cells, suggesting that $CXCR3^+CD4^+$ T cells are imprinted to interact with ICAM-1, if present in the vasculature (Figure 4, C and D). In accordance with these findings in mice, we found that circulating $CXCR3^+CD4^+$ T cells in patients with nonischemic HF had higher expression levels of surface LFA-1 than circulating $CXCR3^-CD4^+$ T cells from the same patients (Figure 4, E and F). Taken together, these data identify CXCR3 and LFA-1 as critical surface molecules expressed in $CD4^+$ T cells of mice and humans with HF, which are likely primed to be recruited to the heart in response to chemotactic signals induced by CXCL9 and CXCL10.

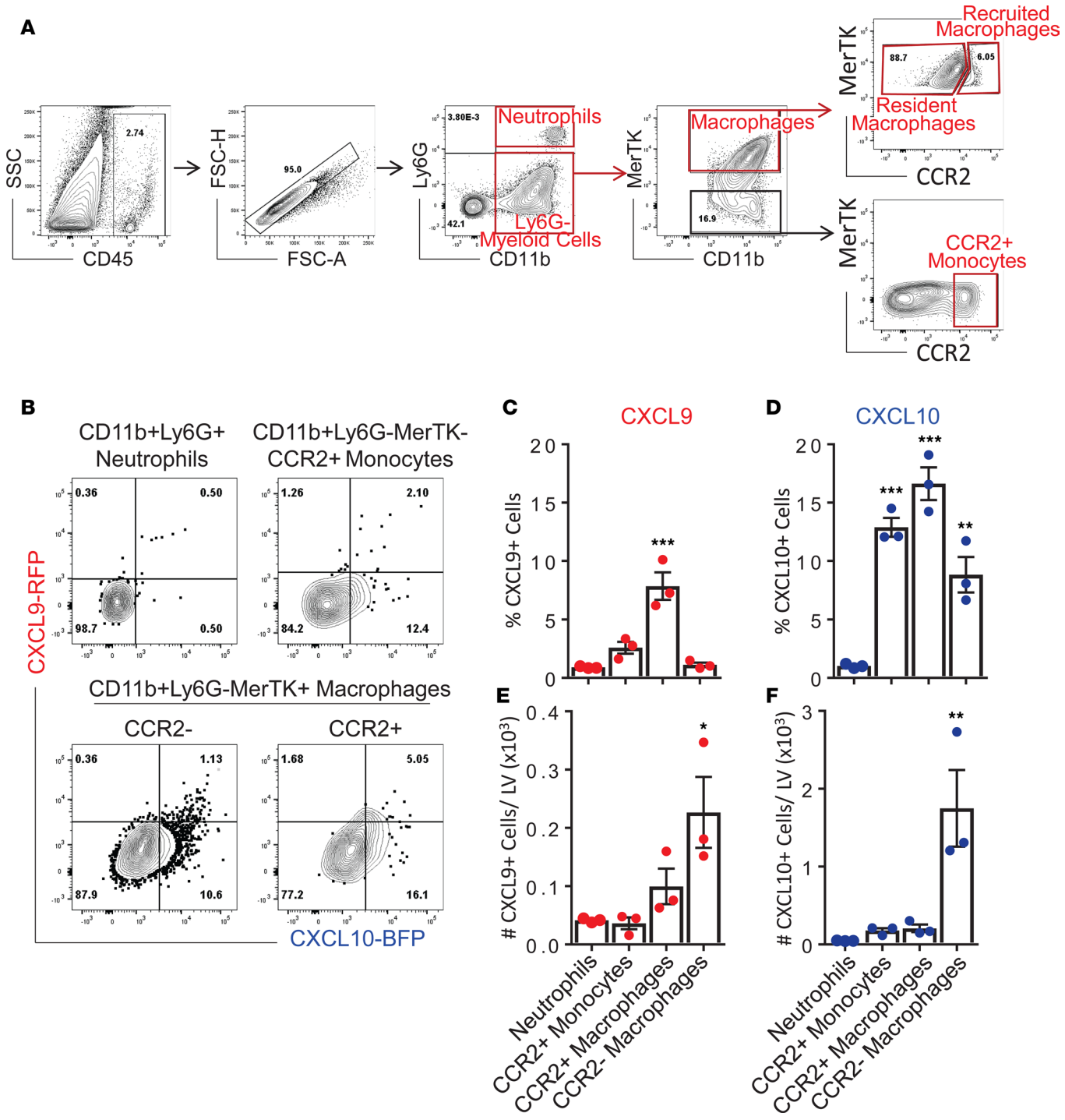

Figure 3. CXCL9 and CXCL10 are produced by resident and recruited cardiac myeloid cells in response to cardiac pressure overload. REX3 mice were subjected to TAC surgery, and LV tissue sections were isolated for analysis of CXCL9 and CXCL10 expression by flow cytometry, 4 weeks after TAC. (**A** and **B**) CD11b⁺Ly6G⁺ Neutrophils, CD11b⁺MerTK⁻CCR2⁺ monocytes, CD11b⁺MerTK⁺CCR2⁻ resident macrophages, and CD11b⁺MerTK⁺CCR2⁺ recruited macrophages were identified by flow cytometry with the indicated gating strategy. (**C–F**) CXCL9 and CXCL10 expression was quantified as frequency (**C** and **D**) and absolute cell number per LV (**E** and **F**). Statistical comparisons are indicated compared with neutrophils. n = 3 mice per group. Error bars represent mean ± SEM (*P < 0.05, **P < 0.01, ***P < 0.001; 1-way ANOVA with Bonferroni post hoc test).

CD4⁺ T cell recruitment to the LV is impaired in Cxcr3⁻/⁻ mice 4 weeks after TAC. To explore the role of CXCR3 chemokine sensing in CD4⁺ T cell recruitment to the LV, we directly compared CD4⁺ T cell responses in WT and *Cxcr3*⁻/⁻ mice. CD4⁺ T cell activation in the mLNs was determined by quantitative flow cytometry at 4 weeks after Sham and TAC surgery. We observed a trend toward lower total numbers of effector CD4⁺

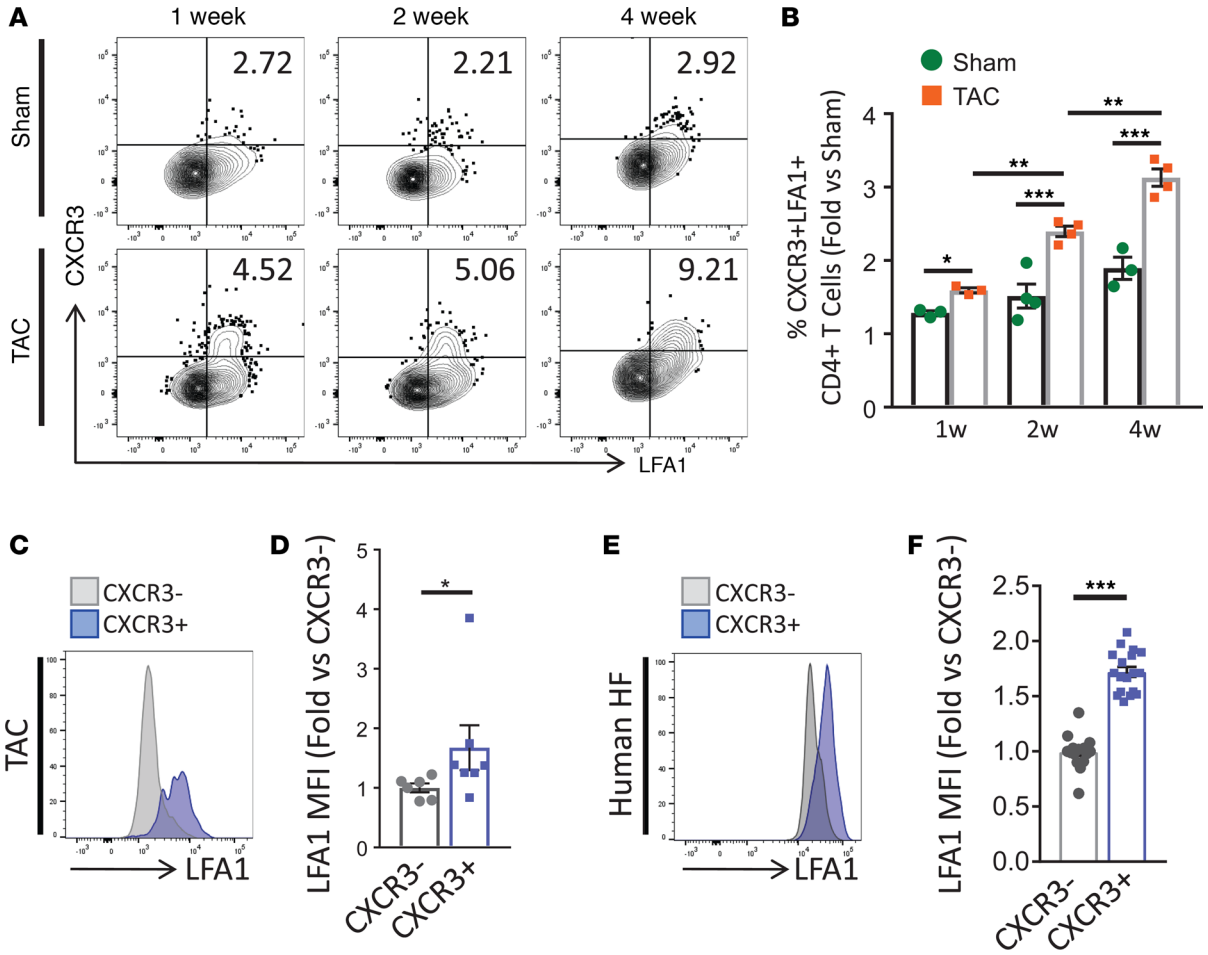

Figure 4. CXCR3⁺CD4⁺ T cells from mice and humans with cardiac pressure overload express high levels of LFA-1. (**A** and **B**) Representative flow cytometry plots (**A**) and quantification (**B**) of CD4⁺ T cells isolated from the mLNs of WT mice at the indicated times after Sham and TAC surgery, indicating surface CXCR3 and LFA-1 expression within the CD4⁺ gate. Relative values to Sham 1 week (w) are indicated. *n* = 3 Sham, 3 TAC 1w; 4 Sham, 4 TAC 2w; 3 Sham, 4 TAC 4w. Error bars represent mean ± SEM (**P* < 0.05, ***P* < 0.01, ****P* < 0.001; 1-way ANOVA with Bonferroni post hoc test). (**C**–**F**) Histogram representation (**C** and **E**) and quantification (**D** and **F**) of LFA-1 expression on CXCR3⁺CD4⁺ and CXCR3⁻CD4⁺ T cells in the mLNs of WT mice 4 weeks after TAC surgery (**C** and **D**) and in peripheral blood of nonischemic HF patients (**E** and **F**). *n* = 7 TAC mice, 20 nonischemic HF patients. Error bars represent mean ± SEM (**P* < 0.05, ***P* < 0.01, ****P* < 0.001; Mann-Whitney unpaired *U* test).

T cells, identified as CD62L^{lo}CD44^{hi}, in the mLNs of *Cxcr3*$^{-/-}$ mice as compared with WT mice at baseline (Sham groups). However, this number was significantly increased in both WT and *Cxcr3*$^{-/-}$ mice 4 weeks after TAC surgery, suggesting that CD4⁺ T cell activation proceeds similarly in the absence of CXCR3 (Figure 5, A and B). Strikingly, the recruitment of CD4⁺ T cells to the LV was significantly impaired in *Cxcr3*$^{-/-}$ mice compared with WT mice in response to TAC, as determined by IHC (Figure 5, C and D). Given our identification of cardiac myeloid resident and recruited cells in the LV as dominant sources of CXCL9 and CXCL10, we next further characterized their presence in *Cxcr3*$^{-/-}$ and WT mice 4 weeks after TAC by quantitative flow cytometry (Figure 5E). Corresponding to our IHC results, the number of CD4⁺ T cells infiltrated in the LV was significantly impaired in *Cxcr3*$^{-/-}$ as compared with WT mice in response to TAC (Figure 5F). In contrast, TAC induced an increase in the overall number of CD11b⁺ myeloid cells infiltrated in the LV, as compared with Sham, that was comparable between both genotypes. More specifically, the total number of CCR2⁺ recruited macrophages was similarly increased in the LV of *Cxcr3*$^{-/-}$ and WT mice in response to TAC, suggesting that the recruitment defect is specific to CD4⁺ T cells (Figure 5, G and H). Moreover, the mRNA expression of *Cxcl9*, as well as its inducer *Ifng*, was significantly lower in the LV of *Cxcr3*$^{-/-}$ mice compared with WT mice after 4 weeks of TAC. Although *Cxcl10* mRNA expression was elevated in the LV of *Cxcr3*$^{-/-}$ mice as compared with Sham controls, this was diminished as compared with WT TAC mice (Figure 5, I–K), suggesting that CD4⁺ T cell recruitment to the LV triggers greater *Cxcl9*

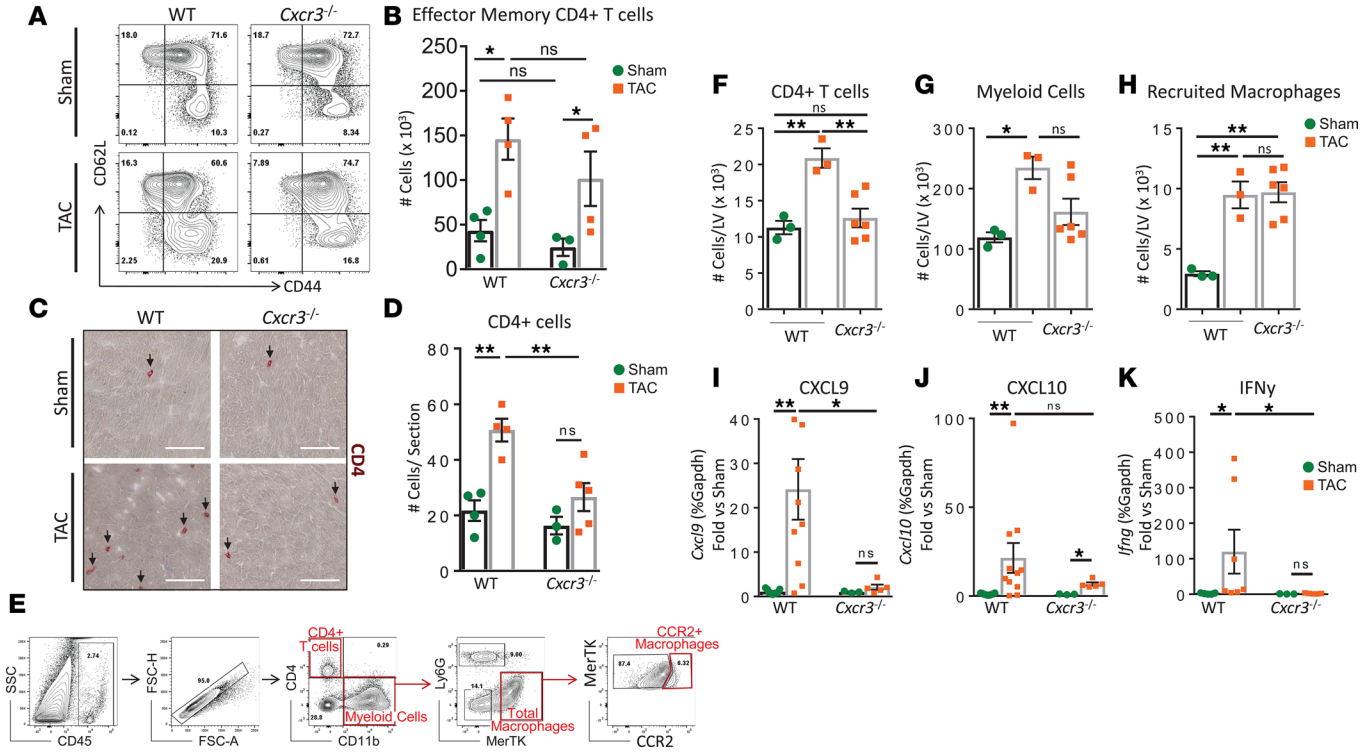

Figure 5. CD4⁺ T cell recruitment to the LV, but not CD4⁺ T cell activation, is impaired in *Cxcr3*$^{-/-}$ mice in response to cardiac pressure overload. CD4⁺ T cells were isolated from the mLN of WT and *Cxcr3*$^{-/-}$ mice, 4 weeks after Sham and TAC surgeries. (**A** and **B**) CD62L^{lo}CD44^{hi} effector CD4⁺ T cells were identified by flow cytometry (**A**) and quantified (**B**). (**C** and **D**) CD4⁺ T cells recruited to the LV were identified by IHC (**C**) and quantified (**D**) per LV section. *n* = 4 Sham, 4 TAC WT; 3 Sham, 5 TAC *Cxcr3*$^{-/-}$. Scale bars: 100 μm. Error bars represent mean ± SEM (**P* < 0.05, ***P* < 0.01; 1-way ANOVA with Bonferroni post hoc test). (**E–H**) The indicated gating strategy shown for WT TAC (**E**) was used to quantify the total cell number per LV of CD4⁺ T cells (**F**), CD11b⁺ myeloid cells (**G**), and CD11b⁺MerTK⁺CCR2⁺ recruited macrophages (**H**) by flow cytometry in WT and *Cxcr3*$^{-/-}$ mice, 4 weeks after Sham and TAC surgeries. *n* = 3 Sham, 3 TAC WT; 6 TAC *Cxcr3*$^{-/-}$ mice. Error bars represent mean ± SEM (**P* < 0.05, ***P* < 0.01; 1-way ANOVA with Bonferroni post hoc test). (**I–K**) mRNA levels in the LV of WT and *Cxcr3*$^{-/-}$ mice at 4 weeks after surgery was determined by qPCR for *Cxcl9* (**I**), *Cxcl10* (**J**), and *Ifng* (**K**). *n* = 9 Sham, 10 TAC WT; 3 Sham, 5 TAC *Cxcr3*$^{-/-}$. Error bars represent mean ± SEM (**P* < 0.05, ***P* < 0.01; 1-way ANOVA with Bonferroni post hoc test).

and *Cxcl10* expression, likely by IFNγ production. Taken together, these data demonstrate that CXCR3 is a central regulator of CD4⁺ T cell recruitment into the heart in response to cardiac pressure overload.

Cxcr3$^{-/-}$ *mice are protected from adverse cardiac remodeling induced by cardiac pressure overload.* We and others have previously shown that CD4⁺ T cell infiltration into the LV is necessary for adverse cardiac remodeling to occur and that Th1 cells specifically drive cardiac fibrosis in response to cardiac pressure overload (4, 5, 21). Thus, we evaluated the extent of LV fibrosis in *Cxcr3*$^{-/-}$ and WT mice, 4 weeks after TAC. While WT mice develop significant perivascular and interstitial fibrosis in response to TAC, we did not identify any signs of LV fibrosis in *Cxcr3*$^{-/-}$ mice (Figure 6, A–D). Moreover, WGA staining of LV tissues revealed that *Cxcr3*$^{-/-}$ mice developed significantly enlarged cardiomyocytes 4 weeks after TAC, but this was significantly attenuated compared with WT mice (Figure 6, E and F). Additionally, the ratio between the mRNA of myosin heavy chain β (*myh7*) and α (*myh6*) isoforms — normally expressed in the fetal and adult hearts, respectively, and an indicator of pathological cardiac hypertrophy — was significantly decreased in *Cxcr3*$^{-/-}$ mice compared with WT mice after TAC (Figure 6G). These data demonstrate that CXCR3 is critical for the development of cardiac fibrosis and partially regulates cardiac hypertrophy induced by cardiac pressure overload due to TAC.

Cxcr3$^{-/-}$ *mice have preserved cardiac function in response to cardiac pressure overload–induced TAC.* We next sought to determine whether the phenotypic changes observed in the heart in *Cxcr3*$^{-/-}$ mice resulted in improved cardiac function by performing noninvasive echocardiography and invasive hemodynamics to comprehensively assess the role of CXCR3 in cardiac function. Transthoracic echocardiography was first used to evaluate LV contractile function. The LV wall and chamber dimensions at the peak of systole and diastole were used to compute fractional shortening and ejection fraction, which were both significantly impaired in WT mice but fully preserved in *Cxcr3*$^{-/-}$ mice, 4 weeks after TAC (Figure 7, A–C).

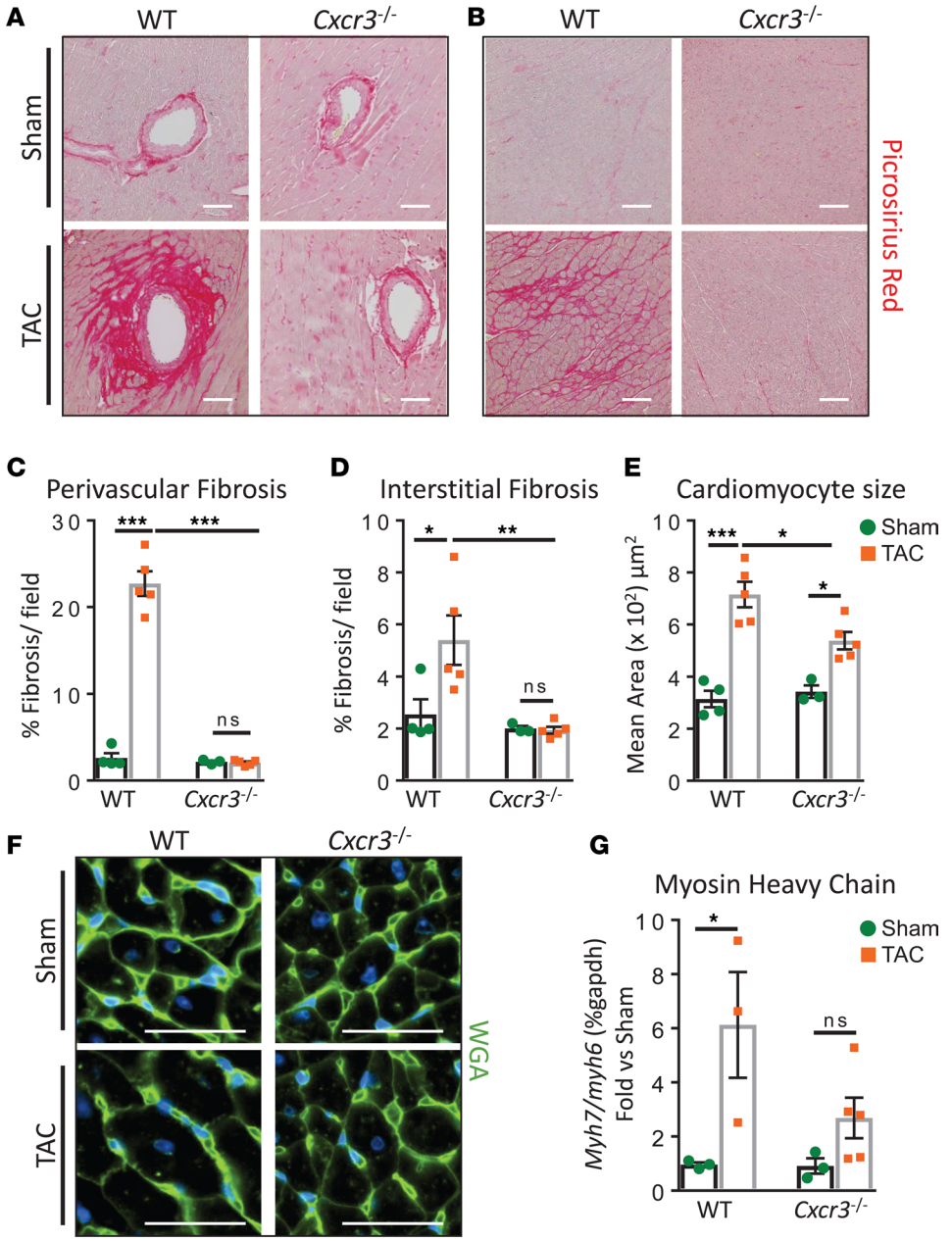

Figure 6. *Cxcr3*$^{-/-}$ mice are protected from adverse cardiac remodeling induced by cardiac pressure overload. LV tissue sections were isolated from WT and *Cxcr3*$^{-/-}$ mice, 4 weeks after Sham and TAC surgeries. IHC was used to determine perivascular fibrosis (**A**) (quantified in **C**) as well as interstitial fibrosis (**B**) (quantified in **D**) by Picrosirius red staining. Scale bars: 100 µm. (**E** and **F**) Mean cardiomyocyte area was quantified by wheat germ agglutinin (WGA) IHC of LV tissue sections (**E**) (as shown in **F**). n = 4 Sham, 5 TAC WT; 3 Sham, 5 TAC *Cxcr3*$^{-/-}$ mice. Scale bars: 50 µm. Error bars represent mean ± SEM (*P < 0.05, ***P < 0.001; 1-way ANOVA with Bonferroni post hoc test). (**G**) The relative LV mRNA expression of the α and β myosin heavy chain isoforms were determined by qPCR to assess pathological cardiomyocyte hypertrophy. n = 3 Sham, 3 TAC WT; 3 Sham, 5 TAC *Cxcr3*$^{-/-}$ mice. Error bars represent mean ± SEM (*P < 0.05; 1-way ANOVA with Bonferroni post hoc test).

Furthermore, LV pressure volume loops were acquired via invasive hemodynamics to monitor cardiac function. Both cardiac contractility (dP/dt max) and relaxation (dP/dt min) indexes were impaired in WT TAC mice but were unchanged in *Cxcr3*$^{-/-}$ TAC mice, despite equally elevated maximum pressures recorded in the LV (Figure 7, D–F, and Table 1). Taken together, these data suggest that CXCR3 is required for cardiac dysfunction associated with impaired CD4$^+$ T cell recruitment and adverse cardiac remodeling in response to cardiac pressure overload.

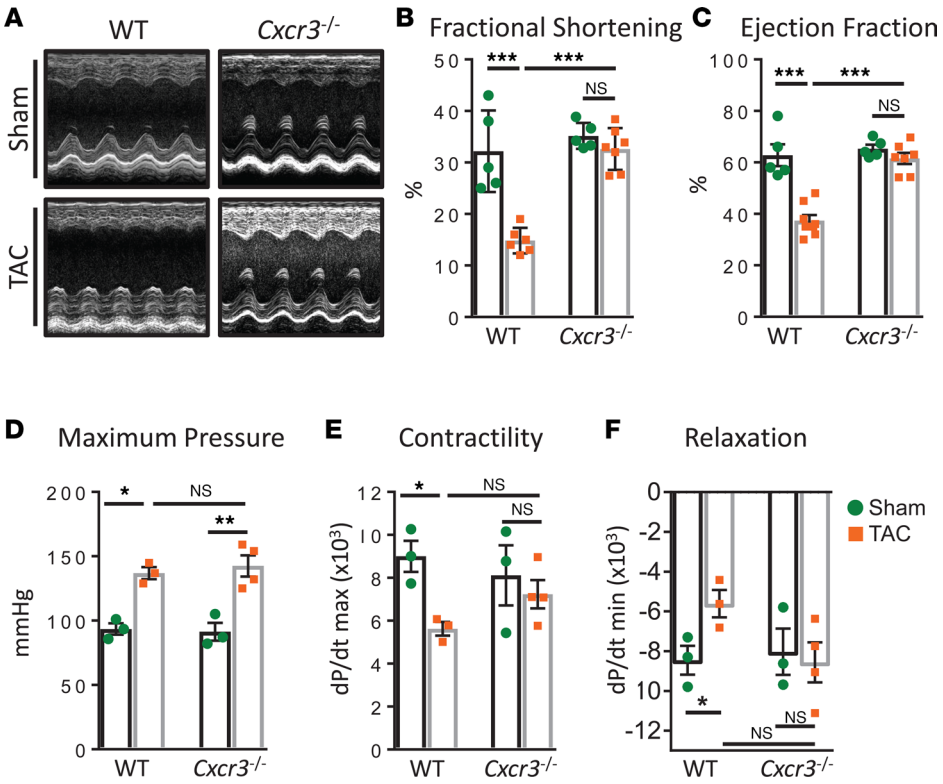

Figure 7. Cardiac function is preserved in *Cxcr3*$^{-/-}$ mice subjected to cardiac pressure overload induced by TAC. (**A–C**) Transthoracic short axis M mode images of the mid LV were acquired by echocardiography (**A**) of WT and *Cxcr3*$^{-/-}$ mice, 4 weeks after Sham and TAC surgeries to quantify fractional shortening (**B**) and ejection fraction (**C**). *n* = 5 Sham, 7 TAC WT; 5 Sham, 7 TAC *Cxcr3*$^{-/-}$ mice. Error bars represent mean ± SEM (***$P < 0.001$; 1-way ANOVA with Bonferroni post hoc test). (**D–F**) Intraventricular hemodynamic measurements were acquired by a pressure volume transducer catheter to quantify maximum LV pressure (**D**), as well as dP/dt max (**E**) and dP/dt min (**F**) as parameters of cardiac contractility and relaxation, respectively. *n* = 3 Sham, 3 TAC WT; 3 Sham, 4 TAC *Cxcr3*$^{-/-}$. Error bars represent mean ± SEM (*$P < 0.05$; 1-way ANOVA with Bonferroni post hoc test).

CXCL9 and CXCL10 induce an increase in Th1 cell adhesion to ICAM-1 under flow conditions in vitro, in a CXCR3- and LFA-1–dependent manner. Our in vivo data indicate that there is a consistent correlation between CXCR3 and LFA-1 expression in CD4$^+$ T cells, both locally in the mLNs of mice and systemically in circulation in HF patients (Figure 4). Furthermore, our data demonstrate that lack of CXCR3 prevents CD4$^+$ T cell recruitment into the LV, cardiac fibrosis, and cardiac dysfunction, supporting a critical role for CXCR3 in CD4$^+$ T cell cardiotropism in response to cardiac pressure overload (Figures 5–7). Previous studies have demonstrated that CXCR3 ligands play a key role in Th1 cell adhesion to endothelial cells under flow conditions in vitro (17) and in vivo using an experimental model of cerebral malaria, and this process was also shown to be dependent on LFA-1 (27, 29). Our in vivo data demonstrate cardiac production of CXCL9 and CXCL10 in the heart in response to TAC (Figures 1–3). Thus, we hypothesized that CXCL9 and/or CXCL10 induce adhesion of Th1 cells to ICAM-1, the major LFA-1 ligand on ECs, as a potential mechanism involved in CXCR3$^+$CD4$^+$ T cell recruitment to the LV in response to cardiac pressure overload. A parallel plate flow chamber apparatus was used to determine chemokine-dependent integrin-mediated adhesion of Th1 cells to immobilized ICAM-1 (30). Accumulation of T cells on ICAM-1 under flow conditions requires activation of the β2 integrin LFA-1, and this can be induced by a variety of agents, including physiological stimulation by chemokines or with phorbol myristate acetate (PMA), an approach that bypasses chemokine receptor signaling (31, 32). As expected, PMA-induced integrin activation led to an increase in Th1 cell adhesion to ICAM-1, and both CXCL9 and CXCL10 also induced an increase in Th1 cell adhesion to ICAM-1 as compared with unstimulated Th1 cells. Interestingly, CXCL9 induced a stronger effect on Th1 cell adhesion to ICAM-1 than CXCL10 (Figure 8, A and B). In all stimulation conditions, Th1 cell adhesion to ICAM-1 was inhibited when Th1 cells were pretreated with a function-blocking antibody to LFA-1 (αLFA-1), confirming the LFA-1 dependence of this adhesion (Figure 8, A and B).

Table 1. Characterization of cardiac function in WT, *Cxcr3*$^{-/-}$, and REX3 mice 4 weeks after Sham or TAC surgery

Parameters	WT Sham	WT TAC	*Cxcr3*$^{-/-}$ Sham	*Cxcr3*$^{-/-}$ TAC	REX3 Sham	REX3 TAC
Total mouse weight (g)/tibia length (mm)	1.60 ± 0.06	1.54 ± 0.03	1.50 ± 0.02	1.46 ± 0.02	1.38 ± 0.03	1.33 ± 0.03
Fractional shortening (%)	32.2 ± 4	16.4 ± 3[A]	35.47 ± 2	33.23 ± 2	37.3 ± 3	26.15 ± 1[A]
Anterior wall thickness (mm)	0.91 ± 0.03	1.16 ± 0.10[A]	0.94 ± 0.02	1.18 ± 0.09[A]	0.74 ± 0.12	1.02 ± 0.08[A]
Posterior wall thickness (mm)	0.88 ± 0.06	1.18 ± 0.09[A]	0.83 ± 0.04	0.93 ± 0.04	0.85 ± 0.13	1.09 ± 0.17[A]
dP/dt min (1 × 10^3) (mmHg/s)	−9.04 ± 0.75	−6.21 ± 0.60[A]	−8.03 ± 1.16	−8.56 ± 1.01	−9.42 ± 1.06	−7.20 ± 0.8[A]
dP/dt max (1 × 10^3) (mmHg/s)	9.01 ± 0.73	5.63 ± 0.32[A]	8.12 ± 1.40	7.23 ± 0.66	8.69 ± 0.34	7.36 ± 0.80

[A]$P < 0.05$, 4 weeks of TAC vs. Sham. Values are means ± SEM.

Th1 cell adhesion to ICAM-1 was also increased with CXCL9 and CXCL10 chemokines immobilized on the coverslip with ICAM-1, mimicking the more physiological expression of chemokines on the apical surface of vessels (Supplemental Figure 1; supplemental material available online with this article; https://doi.org/10.1172/jci.insight.125527DS1). Lastly, we evaluated whether CXCL9 and CXCL10 induction of Th1 cell adhesion to ICAM-1 was dependent on CXCR3 by performing similar assays with *Cxcr3*$^{-/-}$ Th1 cells. PMA stimulation of Th1 cells, which induces T cell LFA-1 activation in a chemokine-independent manner, induced similar levels of Th1 cell adhesion to ICAM-1 in WT and *Cxcr3*$^{-/-}$ cells. However, CXCL9 and CXCL10 failed to induce *Cxcr3*$^{-/-}$ Th1 cell adhesion to ICAM-1, suggesting that CXCL9 and CXCL10 act through CXCR3 to induce WT Th1 cell adhesion to ICAM-1 (Figure 8, C and D). Taken together, these data indicate that CXCL9, and to lesser extent CXCL10, engagement of CXCR3 promote LFA-1 integrin–dependent Th1 cell adhesion to ICAM-1.

Discussion

The results presented in this study using human T cells and heart tissue from patients with nonischemic HF, combined with the mouse experimental model of cardiac pressure overload induced by TAC in WT, *Cxcr3*$^{-/-}$, and REX3 reporter mice, identify a critical role for cardiac CXCL9 and CXCL10, as well as their receptor CXCR3 on CD4$^+$ T cells, as major drivers of CD4$^+$ T cell cardiotropism through mechanisms that implicate CD4$^+$ T adhesion to ICAM-1. Patients with HF present with systemically elevated levels of CXCL9 and CXCL10 (10), enhanced ICAM-1 expression, and significant heart T cell infiltration (4). Here, we establish a CXCL9/CXCL10/CXCR3/ICAM-1 axis regulating T cell cardiotropism and adverse cardiac remodeling in pressure overload–induced cardiac dysfunction.

We report for the first time to our knowledge increased numbers of CXCR3$^+$ leukocytes, the majority of them being CXCR3$^+$ T cells, in the LV of nonischemic end-stage HF patients. Increased numbers of CXCR3$^+$ T cells have been reported in the circulation of patients with nonischemic HF as a result of idiopathic cardiomyopathy and proposed as potential biomarkers to predict HF, although this increase did not involve CXCR3$^+$CD4$^+$ T cells (33). CXCR3$^+$ T cells express higher levels of the integrin LFA-1 and, thus, have the potential to adhere more efficiently to ICAM-1 and infiltrate the heart. While the human observations should be interpreted with caution, they interestingly parallel our observations using the experimental model of pressure overload–induced cardiac dysfunction induced by TAC in mice. Our data demonstrate that TAC induces heart infiltration of CXCR3$^+$CD4$^+$ T cells and that CXCR3$^+$CD4$^+$ T cells display higher levels of LFA-1 as compared with CXCR3$^-$CD4$^+$ T cells in the mLN that drain the heart. These results are in line with a recent study demonstrating CXCR3$^+$ T cell infiltration in mice with cardiac inflammation induced by LPS. In this setting, the receptor of the hepatocyte growth factor (HGF) c-Met was identified as a critical driver of CXCR3$^+$ T cell cardiotropism (34), which was prevented using a function-blocking antibody toward CXCR3. Whether HGF or other tissue factors known to induce chemokine receptors in a tissue-dependent manner (35, 36) are responsible for CD4$^+$ T cell imprinting of CXCR3 in pressure overload–induced cardiac dysfunction requires further investigation.

Our results using reporter mice for CXCL9 and CXCL10 (REX3 mice) are the first demonstration to our knowledge that these 2 CXCR3 protein ligands are expressed in the heart in response to cardiac pressure overload, and they identify cardiac myeloid cells, which include resident and recruited macrophages, and cardiac fibroblasts as the main source. While cardiac fibroblasts produce both chemokines

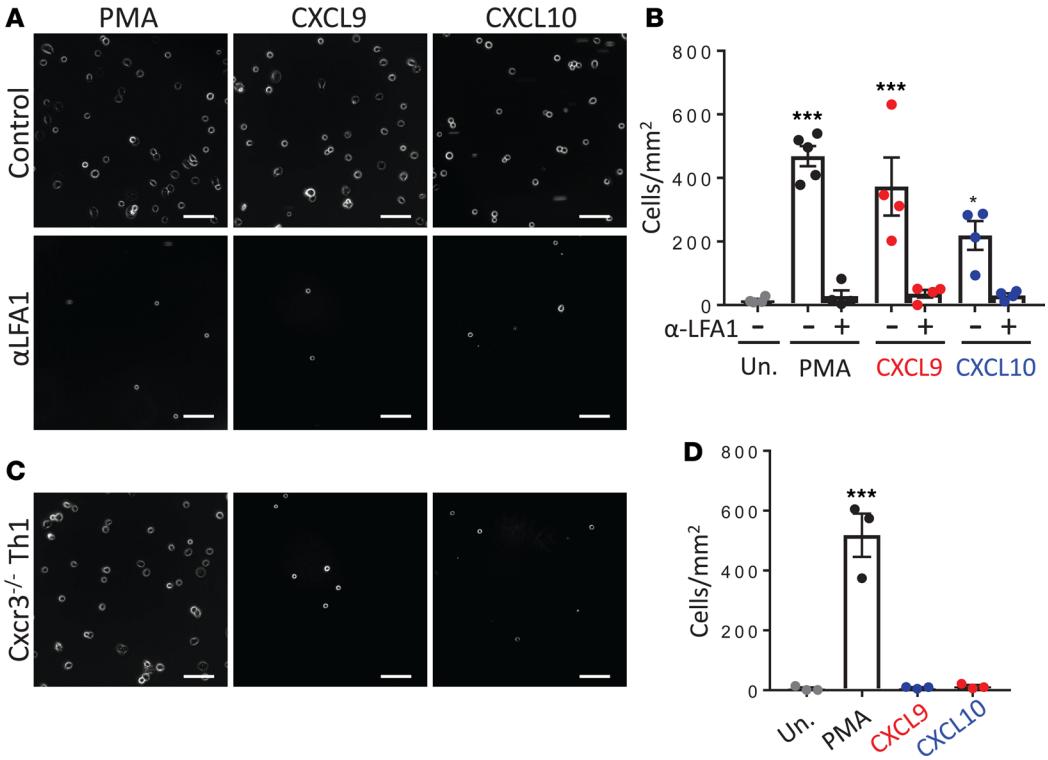

Figure 8. CXCL9 and CXCL10 induce LFA-1–dependent T cell adhesion to ICAM-1 through CXCR3. Naive WT and *Cxcr3*$^{-/-}$ T cells were differentiated in vitro to Th1 cells and treated with either PMA (50 ng/ml), CXCL9 (100 ng/ml), or CXCL10 (100 ng/ml) for 5 minutes at 37°C to induce integrin LFA-1 activation, prior to perfusion over immobilized ICAM-1–coated coverslips at 1 dyne/cm^2 in a parallel plate flow chamber. (**A** and **B**) Representative images (**A**) and quantification (**B**) of real-time videos of WT Th1 cell adhesion to ICAM-1 after treatment with anti–LFA-1 function-blocking antibody or IgG isotype control (20 μg/ml 30 minutes at 37°C). Scale bars: 100 μm. Statistical comparisons are indicated compared with untreated cells. n = 5 independent experiments, analysis of 6 different fields of view per experiment (*P < 0.05, ***P < 0.001; 1-way ANOVA with Bonferroni post hoc test). (**C** and **D**) Representative images (**C**) and quantification (**D**) of real-time videos of *Cxcr3*$^{-/-}$ Th1 cells. Scale bars: 100 μm. Statistical comparisons are indicated compared with untreated cells. n = 3 independent experiments, analysis of 6 different fields of view per experiment. Error bars represent mean ± SEM (***P < 0.001; 1-way ANOVA with Bonferroni post hoc test).

4 weeks after TAC, only myeloid cells produce them earlier (1 week after TAC), demonstrating that the initial source of chemokines preceding T cell infiltration are indeed myeloid cells. Moreover, we report the potentially novel finding that cardiac pressure overload does not induce T cell heart infiltration, adverse cardiac remodeling, and cardiac dysfunction in *Cxcr3*$^{-/-}$ mice. The high expression of CXCL10 mRNA has previously been reported in mice after myocardial infarction (MI) (7), in cardiac allograft rejection (14, 37), and in response to TAC (9), but the protein expression level and the cellular source of chemokine protein is identified here. Interestingly, CXCL10 was demonstrated to be essential in the regulation of the reparative response following MI and appeared to be critical in the recruitment of proinflammatory cells required for healing (7). Similar to our findings in response to cardiac pressure overload, CXCR3$^+$ T cells were significantly increased in the infarcted hearts, correlating with CXCL10 RNA expression. Because T cells are required for tissue repair after ischemia, one logical interpretation is that CXCL10 mediates CXCR3$^+$ T cells infiltration to promote healing. However, a follow-up study demonstrated that the protective effect of CXCL10 after MI was through CXCR3-independent pathways, since *Cxcr3*$^{-/-}$ mice developed similar infarcts and systolic dysfunction as WT mice (15). More recent studies have demonstrated that Th1 cells are not significantly enhanced in the heart in chronic ischemic HF, in contrast to Th17 cells, Th2 cells, and dysfunctional Tregs, which dominate chronic ischemic cardiomyopathy; this supports that the CXCR3–Th1 recruitment axis does not play a role in chronic ischemic HF. (22, 38). In contrast, we and others have demonstrated that T cells are pathogenic and induce adverse cardiac remodeling in response to cardiac pressure overload (4, 5, 21). Our data indicating that *Cxcr3*$^{-/-}$ mice have decreased CD4$^+$ T cell infiltration in the heart and are fully protected from TAC-induced cardiac dysfunction support that, in contrast to chronic

ischemic injury, CXCR3 plays a major role in T cell cardiotropism in pressure overload–induced cardiac dysfunction, along with the previously suggested idea that the effects of CXCR3 in tissue inflammation are dependent on the characteristics of the inflamed organ (14, 39). Our data further demonstrate that, within the same organ (e.g., the heart), the role of CXCR3 depends on the inflammatory trigger itself. Given that the T cell subsets present in the heart in ischemic cardiomyopathy express CCR6 (Th17 cells and Tregs) and CCR4 (Th2 cells), it is likely that their chemokine ligands CCL20 and CCL4, respectively, in contrast to CXCL9 and CXCL10, dominate T cell recruitment in the chronic phase after ischemia and support why *Cxcr3*$^{-/-}$ mice still develop cardiac dysfunction after MI.

Our studies also define the dynamics of CXCR3$^+$CD4$^+$ T cell expansion in the mLNs and the temporal recruitment of CXCR3$^+$CD4$^+$ T cells to the heart in response to cardiac pressure overload. We found that CXCR3$^+$CD4$^+$ T cells are expanded in the mLNs 1 week after induction of cardiac pressure overload and continue to be expanded over time; however, infiltration in the heart does not occur until a week later, as reported previously for CD4$^+$ T cell infiltration (4). Remarkably, CXCR3$^+$CD4$^+$ T cell infiltration in the heart overlaps in time with the highest expression of heart CXCL9 and CXCL10, which is when pathological cardiac remodeling has been described to take place (4, 21). We also found that the cytokine IFNγ, known to induce CXCL9 and CXCL10, was simultaneously upregulated in the heart at the time of CD4$^+$ T cell infiltration and CXCL9 and CXCL10 induction after TAC, peaking at 4 weeks when heart infiltrated CD4$^+$ T cells are present. However, our studies with REX3 mice clearly demonstrate that CD4$^+$ T cells are not the cardiac source of either CXCL9 or CXCL10 and, instead, demonstrate that myeloid cells are the main source and cardiac fibroblast are a secondary source. Myeloid cells that include monocytes and monocyte-derived DCs have indeed been reported to be major producers of CXCL9 and CXCL10 in the inflamed brain (27). Recent studies indicate that CCR2$^+$ myeloid cells precede CD4$^+$ T cell infiltration in the heart in response to TAC, and their depletion results in impaired CD4$^+$ T cell expansion in the mLNs and subsequent recruitment to the heart (40, 41). Our data, in line with these studies, demonstrate that a high percentage of CCR2$^+$-recruited monocytes and macrophages are indeed a source of CXCL10 and that CCR2$^+$ macrophages also produce CXCL9. Moreover, our data identify a significant percentage and absolute number of CCR2$^-$ resident macrophages as major producers of both CXCL9 and CXCL10. These observations, together with our results identifying cardiac fibroblasts as producers of CXCL10 and, to a lesser extent, CXCL9, are potentially novel, as is the finding that endothelial cells, previously identified as producers of both of these chemokines in vitro and in distinct inflammatory settings in vivo (27), are not responsible for chemokine production in the heart in response to cardiac pressure overload. We have previously reported that CD4$^+$IFNγ$^+$ (Th1) cells are major drivers of adverse cardiac remodeling in response to TAC. Moreover, induction of CXCR3 is intertwined with Th1 cell differentiation and controlled by the Th1 cell signature transcription factor T-bet (13, 42). Thus, as CXCR3$^+$CD4$^+$ T cells expand in the mLNs and migrate to the heart in response to chemokines CXCL9 and CXCL10, they can further release IFNγ and, in turn, induce CXCL9 and CXCL10 production by cardiac myeloid cells and cardiac fibroblasts to induce subsequent waves of T cell recruitment in a cycle that contributes to HF progression. Our findings in REX3 mice also indicate that CXCL10 production in the heart is higher than CXCL9. While CXCL9 is mainly induced by IFNγ, CXCL10 expression is also dependent on type I IFN; thus, it is likely that type I IFN signals yet to be described are induced by TAC and contribute to CXCL10 induction and T cell–mediated pathology in pressure overload–induced cardiac dysfunction, similarly to the recently described role for type I IFN signals in cardiac repair after MI (8).

Our in vivo findings demonstrate that the CXCR3$^+$CD4$^+$ T cells expanded in the mLN 1 week after TAC coexpress high levels of total surface LFA-1, compared with CXCR3$^-$CD4$^+$ T cells. Similar findings have been observed in CD4$^+$ T cells in other models of low-grade inflammation, such as high-fat diet–induced metabolic stress (43). However, what induces LFA-1 surface expression on CXCR3$^+$ T cells is unknown. One possibility is that continuous chemokine signaling during cardiac pressure overload results in transcriptional and/or posttranscriptional regulation of the 2 components of LFA-1 (CD11a and CD18), as previously reported during monocyte differentiation (44). An alternative possibility is that signaling through CXCR3 results in LFA-1 translocation from an intercellular pool to the cell surface, as recently described for T cells during antigen presentation (45) and during T cell migration (46). All of these mechanisms could be in place to enhance LFA-1 presence at the CD4$^+$ T cell surface and increase the chances of LFA-1 activation when CXCL9 and/or CXCL10 chemokines are encountered by CXCR3, resulting in adhesion to intramyocardial ICAM-1 and recruitment into the heart. These possibilities of CXCR3 signaling to induce surface LFA-1 warrant future investigation.

In contrast with the less-understood mechanisms that regulate LFA-1 surface expression, the mechanisms of integrin affinity are better understood, and our mechanistic in vitro studies under shear flow conditions support a role for the CXCR3/LFA-1/ICAM-1 adhesion axis that could likely contribute to the role of CXCR3/CXCL9/CXCL10 and ICAM-1/LFA-1 in cardiac pressure overload in vivo. T cells require chemokine signaling to induce Rap-1 activation and subsequent inside-out signals that result in LFA-1 integrin affinity changes that allow optimal adhesion to ICAM-1 (18, 19, 31, 47, 48), and blockade of LFA-1 has been demonstrated to be protective in TAC (49). Our *i*n vitro data using different triggers of integrin activation — such as PMA, which bypasses chemokine receptor signaling, chemokines, and Th1 cells from WT or *Cxcr3*$^{-/-}$ mice — support that CXCL9 and CXCL10 signaling through CXCR3 induces integrin activation, resulting in adhesion to ICAM-1 (Figure 8). Because LFA-1 is the main T cell ligand for endothelial ICAM-1, and because ICAM-1 is induced in the intramyocardial vessels in response to TAC and modulates T cell recruitment (3, 49), our current model is that CXCR3^{+}CD4^{+} T cells are primed in the mLNs to traffic to the heart, where CXCL9 and CXCL10 signals may induce ICAM-1–mediated adhesion. Our results further indicate that CXCL9 induces more LFA-1–dependent Th1 arrest to ICAM-1 than CXCL10. Although in vivo TAC induces less CXCL9 than CXCL10, CXCL9 may be more potent in inducing CXCR3^{+} T cell recruitment to the heart.

Our results using *Cxcr3*$^{-/-}$ TAC mice show a striking lack of heart CD4^{+} T cell infiltration associated with blunted cardiac fibrosis and preserved cardiac dysfunction, suggesting that CXCR3 regulates CD4^{+} T cell trafficking into the heart and adverse cardiac remodeling in response to TAC. Interestingly, myeloid cell recruitment — and, specifically, CCR2^{+} macrophage recruitment — was not impaired in *Cxcr3*$^{-/-}$ mice in response to TAC, suggesting that myeloid cells may be the source of *Cxcl10* transcripts observed in *Cxcr3*$^{-/-}$ mice 4 weeks after TAC. Because the *Cxcl10* transcript levels are decreased as compared with WT mice, our data suggest that a T cell signal may be required for full induction of CXCL10. Whether this signal comes from direct interactions between Th1 cells with myeloid cells, as we have previously described with cardiac fibroblasts (5), or indirectly by cytokine release — likely IFNγ and TNFα, known inducers of both CXCL9 and CXCL10 — requires further investigation. The observed lack of fibrosis may be simply due to the decreased CD4^{+} T cell infiltration driving cardiac fibroblast transformation, as we have previously reported (5); alternatively, it may be due to a delayed recruitment of CXCR3^{+} myofibroblasts, a process previously described during healing after MI (15). Because we use a global *Cxcr3*$^{-/-}$ mouse, there is a possibility that the protection observed from adverse cardiac remodeling and cardiac dysfunction may imply CXCR3 in cells other than Th1 cells, such as cardiac fibroblasts, endothelial cells, or myeloid cells. Nevertheless, given the critical role Th1 cells play in cardiac fibrosis, our results support that lack of CD4^{+} T cell CXCR3 is a major contributor to the observed protection. Our results indicate that cardiac pressure overload induces CD4^{+} T cell activation in *Cxcr3*$^{-/-}$ mice, determined by the number of CD62L^{lo}CD44^{hi}CD4^{+} T cells. This observation somewhat differs from the impaired T cell activation and Th1 differentiation described in the LNs of *Cxcr3*$^{-/-}$ mice induced by exogenous peptide immunization and viral infection in response to stromal CXCL9 and hematopoietic CXCL10 (13). Although individual cell production of IFNγ and TNFα by mLN CD4^{+} T cells was not determined in these in vivo studies, in vitro differentiation of *Cxcr3*$^{-/-}$ Th1 cells was not impaired (Supplemental Figure 2). We interpret these data to suggest that CXCR3 regulation of effector CD62L^{lo}CD44^{hi}CD4^{+} T cell activation may be specific to the antigens triggering the response in the LNs, which are so far unknown in the context or cardiac pressure overload; this is an area of ongoing investigation. In line with our results, CXCR3 has been shown to regulate T cell recruitment to adipose tissue during inflammation, independently of Treg activation in the periphery, although — in this case — the draining LNs were not directly evaluated (50).

In summary, our data demonstrate a role for CXCR3 and its ligands CXCL9 and CXCL10 in mediating CD4^{+} T cell cardiotropism in cardiac pressure overload–induced HF. These results suggest the attractive possibility of potentially targeting CXCR3 therapeutically, a possibility that has been successful in experimental models of Th1-mediated pathologies such as arthritis, encephalomyelitis, and cardiac allograft rejection using a small molecule CXCR3 antagonist (51). Our results, together with the growing body of literature supporting distinct inflammatory and profibrotic responses in different etiologies of HF, enhance our global understanding of cardiac inflammation and its impact in adverse cardiac remodeling and cardiac function. Our results highlight the importance of targeting specific pathways for T cell cardiotropism in a manner that takes into account the initial trigger of cardiac inflammation leading to HF, as opposed to a global antiinflammatory approach common to all etiologies, to achieve therapeutic immunomodulation in HF.

Methods

Human subjects. Venous blood samples were obtained from human subjects with AHA Class A–C nonischemic HF referred for cardiac catheterization as part of their evaluation for heart disease (n = 20). Viable LV free wall tissue from control subjects (n = 3) was obtained from the National Disease Research Interchange (NDRI), and from end-stage HF subjects after LV Assist Device (LVAD) support (n = 3).

Mice. Mice were bred and maintained under pathogen-free conditions at Tufts University animal facilities. C57BL/6 WT, *Cxcr3*$^{-/-}$ (B6.129P2-*Cxcr3*^{tm1Dgen}/J, the Jackson Laboratory), and REX3 mice (provided by A. Luster, Massachusetts General Hospital) were euthanized at 10–14 weeks of age for tissue collection.

Mouse model of TAC. Pressure overload was induced by constricting the transverse aorta of 8- to 10-week-old male mice to induce HF, as previously described (52). Sham-operated mice underwent the same procedure but without aortic ligation. One, 2, and 4 weeks after surgery, mice were euthanized and tissue was harvested for further analysis, as described (3).

qPCR of LV samples. Total RNA was extracted from mouse heart LV tissues directly using Trizol (Invitrogen). RNA was then reverse transcribed to cDNA following Applied Biosystems' protocol using MuLV Reverse Transcriptase and amplified by real-time PCR with SYBR green PCR mix (Applied Biosystems). Samples were quantified in triplicate using 40 cycles performed at 94°C for 30 seconds, 60°C for 45 seconds, and 72°C for 45 seconds using an ABI Prism 7900 Sequence Detection System. Primer sequences: *Tnfa* forward, 5′ - GCA CAG AAA GCA TGA CCC G - 3′, and reverse, 5′ - GCC CCC CAT CTT TTG GG - 3′; *Ifng* forward, 5′ - AAC GCT ACA CAC TGC ATC TTG G - 3′, and reverse, 5′ - GCC GTG GCA GTA ACA GCC - 3′; *cxcl9* forward, 5′ - CTT GAG CCT AGT CGT GAT AAC - 3′, and reverse, 5′ - CCA GCT TGG TGA GGT CTA TC - 3′; *cxcl10* forward, 5′ - ATG ACG GGC CAG TGA GAA TG - 3′, and reverse, 5′ - ATT CTT TTT CAT CGT GGC AAT GA - 3′; and *gapdh* forward, 5′ - ACC ACA GTC CAT GCC ATC AC - 3′, and reverse 5′ - TCC ACC ACC CTG TTG CTG TA - 3′.

Quantitative flow cytometry. Flow cytometry was performed to analyze the immune profile present in response to TAC. The data was acquired on a LSRII (39) and analyzed using FlowJo software. LV digests by collagenase type II (0.895 mg/ml) digestion and lymphoid organs were harvested from Sham and TAC mice and stained with the following monoclonal antibodies (mAbs): FITC-conjugated anti-CD4 (clone GK1.5), APC-Cy7–conjugated anti-CD4 (clone GK1.5), PE- and APC-conjugated anti-CD4 (clone RM4-5), FITC-conjugated anti-CD3e (clone 145-2C11), PE-conjugated anti-CD45.2 (clone 104), APC-conjugated anti-CXCR3 (clone CXCR3-173), FITC-conjugated anti-CD11a (clone 2D7), PE-conjugated anti-IFNγ (clone XMG1.2), FITC-conjugated anti-CD31 (clone MEC13.3), APC-Cy7– and PerCP-conjugated anti-CD11b (clone M1/70), PerCP-Cy5.5–conjugated anti-Ly6G (clone IA8), APC-conjugated anti-MerTK (clone 2B10C42), FITC-conjugated anti-CCR2 (clone SA203G11), APC-conjugated anti-CD44 (clone IM7), and PE-conjugated anti-CD62L (clone MEL-14). All antibodies were purchased from BioLegend. APC-conjugated anti-Feeder Cells (clone mEF-SK4) was purchased from Miltenyi Biotec. Cells were surface stained by incubation with the relevant antibodies diluted in PBS + 2% FBS for 20 minutes at room temperature, followed by 2 washes with PBS 2% FBS. When intracellular staining of signature cytokines was performed, cell suspensions were initially incubated for 3–5 hours at 37°C with RPMI T cell media containing 0.1% ionomycin (MilliporeSigma, I0634), 0.1% brefeldin A (BioLegend, 420601), 0.1% monensin (BioLegend, 420701), and 50 ng/ml of PMA (MilliporeSigma, P8139). After the incubation, surface staining was performed as indicated above, followed by cell fixation for 20 minutes at room temperature in light-protected storage with Fixation buffer (BD Biosciences, 554655). Upon fixation and being washed with PBS 2% FBS, cell suspension was permeabilized with 1× wash/permeabilization buffer (BD Biosciences, 554723; diluted in distilled water) and intracellular stained for 20 minutes at room temperature in light-protected storage. Absolute cell numbers were quantified using Precision Count Beads (BioLegend).

Histology. Human LV tissues were fixed in 10% formalin, embedded in paraffin, and cut into 5-μm sections. IHC with primary antibody against human CXCR3 (LSBio, catalog LS-B10183) was performed for 1 hour (1:100 dilution) followed by incubation with biotinylated goat anti-rabbit secondary antibody (Jackson ImmunoResearch, catalog 111-065-003). Immunofluorescence was performed using anti-CXCR3 (LSBio) (1:100 dilution) and anti-CD3 (Agilent Dako, clone F7.2.38) (1:50 dilution) overnight at 4°C, followed by incubation with Alexa Flour 488–conjugated anti-rabbit (Invitrogen, catalog A-11008) and Alexa Flour 568–conjugated anti-mouse secondary antibodies (Abcam, catalog ab175473). Picrosirius red staining was performed as previously described (4). IHC was performed in mouse LV frozen

sections with primary antibody against murine CD4 (BioLegend, clone GK1.5) for 1 hour (1:500 dilution), followed by incubation with secondary antibody goat anti-rat (Jackson ImmunoResearch, catalog 112-065-062), biotinylated as described (3, 4). For REX3 reporter fluorescence, lightly fixed LV frozen sections were analyzed for immunofluorescence using anti-CD45 (BioLegend, clone 30-F11) and anti-CD31 (BioLegend, clone MEC13.3) for 1 hour (1:500 dilution), followed by incubation with Alexa Flour 488–conjugated anti-rat secondary antibody (Invitrogen, catalog A-21208). FITC-conjugated WGA (Milipore Sigma, catalog L4895) was used at 5 μg/ml. Cardiomyocyte cross-sectional area was quantified by tracing the outline of at least 25 myocytes per section with NIS-Elements software (4). Quantification of percent fibrotic area was performed using NIH ImageJ software. All analyses were performed blindly.

Preparation of effector T cells. $CD4^+$ cells were isolated from spleen cell suspensions of WT or *Cxcr3*$^{-/-}$ mice by positive selection with magnetic beads (Miltenyi Biotec). Naive $CD4^+$ T cells were differentiated into Th1 cells by stimulation with anti-CD3 (BioLegend, clone 17A2) (5 μg/ml) and anti-CD28 (BioLegend, clone 37.51) (1 μg/ml) in the presence of IL-12 (0.01 μg/ml), IL-2 (25U/mL), and anti–IL-4 (BioLegend, clone 11B11) (0.5 μg/ml). On day 3 of stimulation, Th1 cultures were split 1:1 with fresh medium containing IL-2 (25 U/ml). Differentiated T cells were harvested on day 4 and immediately used for experiments. Both WT and *Cxcr3*$^{-/-}$ Th1 cells were equivalently generated in vitro as determined by IFNγ production upon PMA/ionomycin stimulation, and they expressed similar levels of total surface LFA-1 (Supplemental Figure 2).

Measurement of interactions of effector T cells with ICAM-1 under defined flow conditions in vitro. Th1 or Th17 cell interactions with immobilized ICAM-1 were observed by videomicroscopy (×20 objective) under defined laminar flow conditions in a parallel plate apparatus using Nikon NIS-Elements software. Interactions of T cells with immobilized ICAM-1 (8 μg) were measured in 6 different fields of view after the initial minute of each flow rate (shear 1 dyne/cm^2). Where indicated, T cells were stimulated with either PMA (50 ng/ml), CXCL9 (100 ng/ml), or CXCL10 (100 ng/ml) for 5 minutes at 37°C before T cells were perfused in the flow chamber. For LFA-1 blocking, T cells were incubated for 30 minutes with 40 μg/ml αLFA-1 (BioLegend, clone M17/4) at 37°C, prior to the chemokine stimulation. When the immobilized ICAM-1 was incubated with the chemokines, CXCL9 or CXCL10 (2 μg/ml) were added on the coverslip for 15 minutes at 37°C, before the coverslip containing the immobilized protein was placed in the parallel plate apparatus.

In vivo echocardiography. In vivo transthoracic echocardiography was assessed in lightly sedated mice, as described (53). M-mode and 2-dimensional images were obtained from the short-axis view (54). All analyses were performed blindly.

Hemodynamics. A pressure volume transducer catheter was introduced into the LV through the carotid artery of anesthetized mice and used to assess LV function, as previously described (53). Absolute volume was calibrated by the saline injection parallel conductance method, and data were evaluated at steady state (53). Data were digitized and analyzed using custom software (EMKA version 2.1.10).

Statistics. Data were analyzed using GraphPad Prism software and presented as the mean ± SEM. Statistical analyses were done by Mann-Whitney nonparametric unpaired, 2-tailed *U* test when comparing 2 groups. Multiple group comparisons were performed by 1-way ANOVA with Bonferroni post hoc test where indicated. Differences were considered statistically significant at $*P \le 0.05$, $**P \le 0.01$, $***P \le 0.001$.

Study approval. All animal studies were approved by the Tufts University IACUC. Human studies were approved by Tufts University IRB, and all subjects gave written informed consent for participation. Mice were bred and maintained under pathogen-free conditions at Tufts University animal facilities and were treated in compliance with the *Guide for the Care and Use of Laboratory Animals* (National Academies Press, 2011).

Author contributions

NN and AMS designed and conducted experiments, analyzed data, and wrote the manuscript. FV and TN conducted experiments. MA performed the TAC surgery and catheterization for hemodynamic studies. AL recruited and consented patients and collected blood samples. GSH and ADL intellectually contributed to data analysis. PA overviewed the design and interpretation of all studies and wrote the manuscript.

Acknowledgments

These studies were supported by NIH RO1 HL123658 (PA), NIH T32 HL 69770 (TN), NIH T32AI007077-34 and NIH F31HL140883 (NN), and HL123658-01S1 (FV).

Address correspondence to: Pilar Alcaide, Department of Immunology, Tufts University School of Medicine, 136 Harrison Avenue, M&V 701, Boston, Massachusetts 02111, USA. Phone: 617.636.2192; Email: pilar.alcaide@tufts.edu.

1. Braunwald E. Heart failure. *JACC Heart Fail*. 2013;1(1):1–20.
2. Writing Group Members, et al. Heart Disease and Stroke Statistics-2016 Update: A Report From the American Heart Association. *Circulation*. 2016;133(4):e38–360.
3. Salvador AM, et al. Intercellular Adhesion Molecule 1 Regulates Left Ventricular Leukocyte Infiltration, Cardiac Remodeling, and Function in Pressure Overload-Induced Heart Failure. *J Am Heart Assoc*. 2016;5(3):e003126.
4. Nevers T, et al. Left Ventricular T-Cell Recruitment Contributes to the Pathogenesis of Heart Failure. *Circ Heart Fail*. 2015;8(4):776–787.
5. Nevers T, et al. Th1 effector T cells selectively orchestrate cardiac fibrosis in nonischemic heart failure. *J Exp Med*. 2017;214(11):3311–3329.
6. Patel B, Ismahil MA, Hamid T, Bansal SS, Prabhu SD. Mononuclear Phagocytes Are Dispensable for Cardiac Remodeling in Established Pressure-Overload Heart Failure. *PLoS ONE*. 2017;12(1):e0170781.
7. Bujak M, et al. Induction of the CXC chemokine interferon-gamma-inducible protein 10 regulates the reparative response following myocardial infarction. *Circ Res*. 2009;105(10):973–983.
8. King KR, et al. IRF3 and type I interferons fuel a fatal response to myocardial infarction. *Nat Med*. 2017;23(12):1481–1487.
9. Altara R, Gu YM, Struijker-Boudier HA, Thijs L, Staessen JA, Blankesteijn WM. Left Ventricular Dysfunction and CXCR3 Ligands in Hypertension: From Animal Experiments to a Population-Based Pilot Study. *PLoS ONE*. 2015;10(10):e0141394.
10. Altara R, et al. CXCL10 Is a Circulating Inflammatory Marker in Patients with Advanced Heart Failure: a Pilot Study. *J Cardiovasc Transl Res*. 2016;9(4):302–314.
11. Yin WH, et al. The prognostic value of circulating soluble cell adhesion molecules in patients with chronic congestive heart failure. *Eur J Heart Fail*. 2003;5(4):507–516.
12. Franssen C, et al. Myocardial Microvascular Inflammatory Endothelial Activation in Heart Failure With Preserved Ejection Fraction. *JACC Heart Fail*. 2016;4(4):312–324.
13. Groom JR, et al. CXCR3 chemokine receptor-ligand interactions in the lymph node optimize CD4+ T helper 1 cell differentiation. *Immunity*. 2012;37(6):1091–1103.
14. Groom JR, Luster AD. CXCR3 ligands: redundant, collaborative and antagonistic functions. *Immunol Cell Biol*. 2011;89(2):207–215.
15. Saxena A, et al. CXCR3-independent actions of the CXC chemokine CXCL10 in the infarcted myocardium and in isolated cardiac fibroblasts are mediated through proteoglycans. *Cardiovasc Res*. 2014;103(2):217–227.
16. Paust HJ, et al. CXCR3+ Regulatory T Cells Control TH1 Responses in Crescentic GN. *J Am Soc Nephrol*. 2016;27(7):1933–1942.
17. Curbishley SM, Eksteen B, Gladue RP, Lalor P, Adams DH. CXCR 3 activation promotes lymphocyte transendothelial migration across human hepatic endothelium under fluid flow. *Am J Pathol*. 2005;167(3):887–899.
18. Piali L, et al. The chemokine receptor CXCR3 mediates rapid and shear-resistant adhesion-induction of effector T lymphocytes by the chemokines IP10 and Mig. *Eur J Immunol*. 1998;28(3):961–972.
19. D'Ambrosio D, Albanesi C, Lang R, Girolomoni G, Sinigaglia F, Laudanna C. Quantitative differences in chemokine receptor engagement generate diversity in integrin-dependent lymphocyte adhesion. *J Immunol*. 2002;169(5):2303–2312.
20. Taub DD, et al. Recombinant human interferon-inducible protein 10 is a chemoattractant for human monocytes and T lymphocytes and promotes T cell adhesion to endothelial cells. *J Exp Med*. 1993;177(6):1809–1814.
21. Laroumanie F, et al. CD4+ T cells promote the transition from hypertrophy to heart failure during chronic pressure overload. *Circulation*. 2014;129(21):2111–2124.
22. Bansal SS, et al. Activated T Lymphocytes are Essential Drivers of Pathological Remodeling in Ischemic Heart Failure. *Circ Heart Fail*. 2017;10(3):e003688.
23. Tager AM, et al. Inhibition of pulmonary fibrosis by the chemokine IP-10/CXCL10. *Am J Respir Cell Mol Biol*. 2004;31(4):395–404.
24. Ooi JY, et al. HDAC inhibition attenuates cardiac hypertrophy by acetylation and deacetylation of target genes. *Epigenetics*. 2015;10(5):418–430.
25. Altara R, et al. Improving membrane based multiplex immunoassays for semi-quantitative detection of multiple cytokines in a single sample. *BMC Biotechnol*. 2014;14:63.
26. Sierro F, et al. Disrupted cardiac development but normal hematopoiesis in mice deficient in the second CXCL12/SDF-1 receptor, CXCR7. *Proc Natl Acad Sci USA*. 2007;104(37):14759–14764.
27. Sorensen EW, et al. CXCL10 stabilizes T cell-brain endothelial cell adhesion leading to the induction of cerebral malaria. *JCI Insight*. 2018;3(8):e98911.
28. Pinto AR, et al. Revisiting Cardiac Cellular Composition. *Circ Res*. 2016;118(3):400–409.
29. Swanson PA, et al. CD8+ T Cells Induce Fatal Brainstem Pathology during Cerebral Malaria via Luminal Antigen-Specific Engagement of Brain Vasculature. *PLoS Pathog*. 2016;12(12):e1006022.
30. Ye F, Kim C, Ginsberg MH. Reconstruction of integrin activation. *Blood*. 2012;119(1):26–33.
31. Dransfield I, Cabañas C, Craig A, Hogg N. Divalent cation regulation of the function of the leukocyte integrin LFA-1. *J Cell Biol*. 1992;116(1):219–226.
32. Dustin ML, Springer TA. T-cell receptor cross-linking transiently stimulates adhesiveness through LFA-1. *Nature*. 1989;341(6243):619–624.
33. Athanassopoulos P, Vaessen LM, Balk AH, Weimar W, Sharma HS, Bogers AJ. Altered chemokine receptor profile on circulating leukocytes in human heart failure. *Cell Biochem Biophys*. 2006;44(1):83–101.
34. Komarowska I, et al. Hepatocyte Growth Factor Receptor c-Met Instructs T Cell Cardiotropism and Promotes T Cell Migration to the Heart via Autocrine Chemokine Release. *Immunity*. 2015;42(6):1087–1099.

35. McCully ML, Ladell K, Hakobyan S, Mansel RE, Price DA, Moser B. Epidermis instructs skin homing receptor expression in human T cells. *Blood*. 2012;120(23):4591–4598.
36. Mora JR, et al. Selective imprinting of gut-homing T cells by Peyer's patch dendritic cells. *Nature*. 2003;424(6944):88–93.
37. Melter M, et al. Expression of the chemokine receptor CXCR3 and its ligand IP-10 during human cardiac allograft rejection. *Circulation*. 2001;104(21):2558–2564.
38. Bansal SS, et al. Dysfunctional and Proinflammatory Regulatory T-Lymphocytes Are Essential for Adverse Cardiac Remodeling in Ischemic Cardiomyopathy. *Circulation*. 2019;139(2):206–221.
39. Yates CC, et al. Delayed and deficient dermal maturation in mice lacking the CXCR3 ELR-negative CXC chemokine receptor. *Am J Pathol*. 2007;171(2):484–495.
40. Patel B, et al. CCR2+ Monocyte-Derived Infiltrating Macrophages Are Required for Adverse Cardiac Remodeling During Pressure Overload. *JACC Basic Transl Sci*. 2018;3(2):230–244.
41. Hirako IC, et al. Splenic differentiation and emergence of CCR5+CXCL9+CXCL10+ monocyte-derived dendritic cells in the brain during cerebral malaria. *Nat Commun*. 2016;7:13277.
42. Taqueti VR, et al. T-bet controls pathogenicity of CTLs in the heart by separable effects on migration and effector activity. *J Immunol*. 2006;177(9):5890–5901.
43. Mauro C, et al. Obesity-Induced Metabolic Stress Leads to Biased Effector Memory CD4+ T Cell Differentiation via PI3K p110δ-Akt-Mediated Signals. *Cell Metab*. 2017;25(3):593–609.
44. Back AL, Gollahon KA, Hickstein DD. Regulation of expression of the leukocyte integrin CD11a (LFA-1) molecule during differentiation of HL-60 cells along the monocyte/macrophage pathway. *J Immunol*. 1992;148(3):710–714.
45. Capece T, et al. A novel intracellular pool of LFA-1 is critical for asymmetric CD8+ T cell activation and differentiation. *J Cell Biol*. 2017;216(11):3817–3829.
46. Samuelsson M, et al. RhoB controls the Rab11-mediated recycling and surface reappearance of LFA-1 in migrating T lymphocytes. *Sci Signal*. 2017;10(509):eaai8629.
47. Shamri R, et al. Lymphocyte arrest requires instantaneous induction of an extended LFA-1 conformation mediated by endothelium-bound chemokines. *Nat Immunol*. 2005;6(5):497–506.
48. Pasvolsky R, et al. RhoA is involved in LFA-1 extension triggered by CXCL12 but not in a novel outside-in LFA-1 activation facilitated by CXCL9. *J Immunol*. 2008;180(5):2815–2823.
49. Yoshida Y, et al. p53-Induced inflammation exacerbates cardiac dysfunction during pressure overload. *J Mol Cell Cardiol*. 2015;85:183–198.
50. Rocha VZ, et al. CXCR3 controls T-cell accumulation in fat inflammation. *Arterioscler Thromb Vasc Biol*. 2014;34(7):1374–1381.
51. Jenh CH, et al. A selective and potent CXCR3 antagonist SCH 546738 attenuates the development of autoimmune diseases and delays graft rejection. *BMC Immunol*. 2012;13:2.
52. Rockman HA, et al. Segregation of atrial-specific and inducible expression of an atrial natriuretic factor transgene in an in vivo murine model of cardiac hypertrophy. *Proc Natl Acad Sci USA*. 1991;88(18):8277–8281.
53. Blanton RM, et al. Protein kinase g iα inhibits pressure overload-induced cardiac remodeling and is required for the cardioprotective effect of sildenafil in vivo. *J Am Heart Assoc*. 2012;1(5):e003731.
54. Patten RD, et al. 17 Beta-estradiol differentially affects left ventricular and cardiomyocyte hypertrophy following myocardial infarction and pressure overload. *J Card Fail*. 2008;14(3):245–253.